Spin Dynamics of Photogenerated Triradicals in Fixed Distance Electron Donor−Chromophore−Acceptor−TEMPO Molecules

Qixi Mi, Erin T. Chernick, David W. McCamant, Emily A. Weiss, Mark A. Ratner,* and Michael R. Wasielewski*

Department of Chemistry and International Institute for Nanotechnology, Northwestern University, Evanston, Illinois 60208-3113

Received: February 26, 2006; In Final Form: April 21, 2006

The stable free radical 2,2,6,6-tetramethylpiperidinoxyl (TEMPO, T$^{\bullet}$) was covalently attached to the electron acceptor in a donor−chromophore−acceptor (D−C−A) system, MeOAn−6ANI−Ph$_n$−A−T$^{\bullet}$, having well-defined distances between each component, where MeOAn = *p*-methoxyaniline, 6ANI = 4-(*N*-piperidinyl)-naphthalene-l,8-dicarboximide, Ph = 2,5-dimethylphenyl (n = 0,1), and A = naphthalene-1,8:4,5-bis(dicarboximide) (NI) or pyromellitimide (PI). Using both time-resolved optical and EPR spectroscopy, we show that T$^{\bullet}$ influences the spin dynamics of the photogenerated triradical states ^{2,4}(MeOAn$^{+\bullet}$−6ANI−Ph$_n$−A$^{-\bullet}$−T$^{\bullet}$), resulting in modulation of the charge recombination rate within the triradical compared with the corresponding biradical lacking T$^{\bullet}$. The observed spin−spin exchange interaction between the photogenerated radicals MeOAn$^{+\bullet}$ and A$^{-\bullet}$ is not altered by the presence of T$^{\bullet}$, which interacts most strongly with A$^{-\bullet}$ and accelerates radical pair intersystem crossing. Charge recombination within the triradicals results in the formation of ^{2,4}(MeOAn−6ANI−Ph$_n$−^{3*}NI−T$^{\bullet}$) or ^{2,4}(MeOAn−^{3*}6ANI−Ph$_n$−PI−T$^{\bullet}$) in which T$^{\bullet}$ is strongly spin polarized in emission. Normally, the spin dynamics of correlated radical pairs do not produce a net spin polarization; however, the rate at which the net spin polarization appears on T$^{\bullet}$ closely follows the photogenerated radical ion pair decay rate. This effect is attributed to antiferromagnetic coupling between T$^{\bullet}$ and the local triplet state ^{3*}NI, which is populated following charge recombination. These results are explained using a switch in the spin basis set between the triradical and the three-spin charge recombination product having both T$^{\bullet}$ and ^{3*}NI or ^{3*}6ANI present.

Introduction

Controlling the lifetimes of photoinduced radical ion pairs is important for developing molecular materials for electronics, photonics, and spintronics.[1−16] We have developed several methods for controlling charge transport in organic donor−chromophore−acceptor (D−C−A) triads using multiple ultrafast laser pulses to manipulate the course of electron-transfer reactions.[17−19] Building on this work, we are now exploring the use of spin dynamics to control charge and spin transport properties within D−C−A molecules. Photogenerated radical pairs are capable of exhibiting coherent spin motion over microsecond time scales,[20,21] which is considerably longer than coherent phenomena involving photogenerated excited states. This affords the possibility that coherent spin motion can provide the basis for novel organic computational devices.[22−31] A greater fundamental understanding of the factors controlling spin dynamics in complex organic donor−acceptor systems is necessary to achieve this goal.

The rate of radical pair intersystem crossing (RP-ISC) between photogenerated singlet and triplet radical pairs (RPs) has been shown to increase in the presence of stable free radicals and triplet state molecules.[32−36] In some of these systems, the photoinduced RP is covalently linked to the stable radical using a flexible connection, which results in a broad distribution of distances and spin−spin interaction strengths that make the analysis of the spin dynamics difficult.[37−40] We have addressed this problem by rigidly attaching a stable radical to a donor−acceptor system having restricted distances and orientations between all molecular components. We recently showed that covalently attaching a 2,2,6,6-tetramethylpiperidinoxyl (TEMPO, T$^{\bullet}$) stable free radical to the acceptor of a rigid D−C−A molecule perturbs charge recombination rates via an enhanced intersystem crossing (EISC) mechanism similar to that observed for intermolecular systems,[32,33,35] while not altering the spin−spin exchange interaction within the photogenerated radical ion pair.[41] Given these encouraging results, we have expanded our studies of how the spin dynamics of D−C−A triads are influenced by the presence of a third spin attached specifically to the electron acceptor at a relatively close distance.

The spin density distribution of T$^{\bullet}$ is localized largely on its N−O group and not on the molecule to which T$^{\bullet}$ is appended,[42,43] so that attachment of T$^{\bullet}$ to A within the triad does not result in significant spin delocalization onto A itself. We have modified the well-characterized D−C−A triad system, MeOAn−6ANI−Ph$_n$−NI (or PI), **1a**−**4a**,[41,44,45] where MeOAn = *p*-methoxyaniline, 6ANI = 4-(*N*-piperidinyl)naphthalene-1,8-dicarboximide, Ph = 2,5-dimethylphenyl (n = 0, 1), NI = naphthalene-1,8:4,5-bis(dicarboximide), and PI = pyromellitimide to probe the spin dynamics of the photogenerated three-spin system (Scheme 1). We have demonstrated that photoexcitation of D−C−A triads **1a**−**4a** with 416-nm light results in a two-step charge separation (CS) to form a singlet radical ion pair (RP_S), which undergoes radical pair intersystem crossing (RP-ISC) to the corresponding triplet radical ion pair (RP_T).[41,45−47] Charge recombination (CR) can occur either from RP_S to the ground state or from the RP_T to the lowest neutral triplet state. We have now synthesized analogues of this system: MeOAn−6ANI−Ph$_n$−NI(or PI)−T$^{\bullet}$, **1b**−**4b**, in which the stable T$^{\bullet}$ radical is attached to the terminal *N*-imide of either the NI or PI acceptors. The resulting molecules position T$^{\bullet}$ at a fixed distance and orientation relative to each electron donor and acceptor

* To whom correspondence should be addressed. E-mail: m-wasielewski@northwestern.edu.

10.1021/jp061218w CCC: $33.50
Published on Web 05/24/2006

SCHEME 1

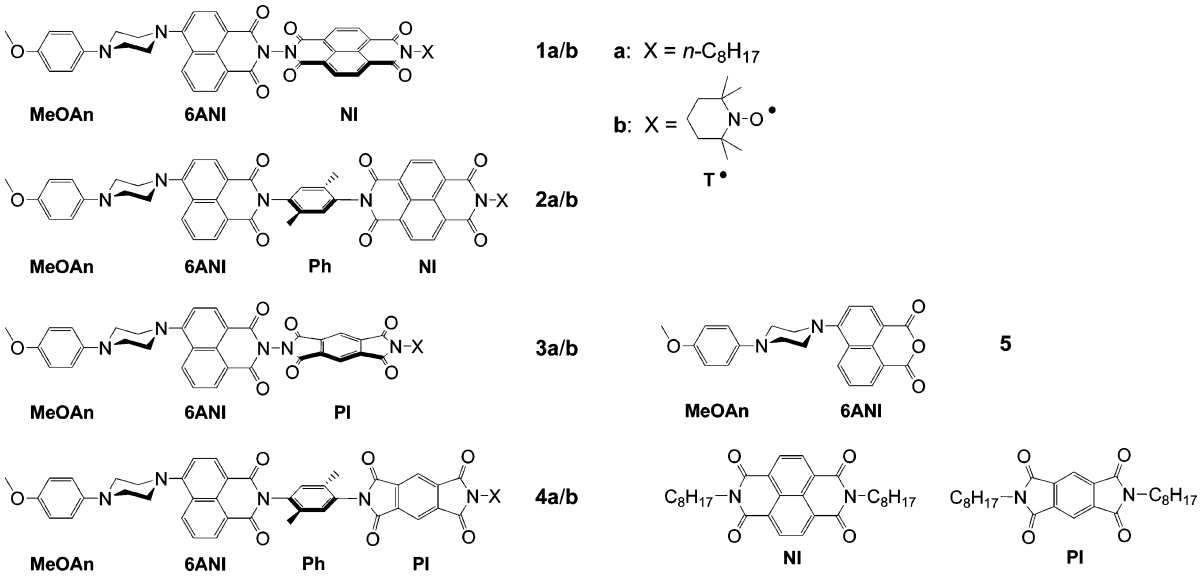

within the triad. The spin dynamics of the photogenerated triradicals are studied using magnetic field effects on the triplet yields following CR as well as time-resolved electron paramagnetic resonance spectroscopy (TREPR).

Experimental Section

The synthesis and characterization of compounds **1a**−**4a**, **1b**, and **3b** have been reported previously,[41,45] and those of **2b** and **4b** can be found in the Supporting Information. Samples were purified for spectroscopy by preparative thin-layer chromatography and stored for at most 7 days at 4 °C until measurements were performed. All solvents were spectrophotometric grade or distilled prior to use.

Cyclic voltammetry measurements were performed in butyronitrile solutions containing 0.1 M tetra-*n*-butylammonium perchlorate (TBAP) electrolyte using a CH Model 622 electrochemical work station. A 1.0-mm diameter Pt disk electrode, Pt wire counter electrode, and Ag/Ag_xO reference electrode were employed. The ferrocene/ferrocinium couple (Fc/Fc^+, 0.52 V vs SCE) was used as an internal reference for all measurements.

Ground-state absorption measurements were made on a Shimadzu (UV-1601) spectrophotometer. Sample solutions were prepared in toluene, transferred to a sealable cuvette, degassed by three freeze−pump−thaw cycles and then kept under vacuum throughout each spectroscopic run. The optical density at the pump wavelength was 0.4−0.6 per 2-mm path length for femtosecond transient absorption (TA) experiments and 0.8−1.0 per 1-cm path length for nanosecond transient absorption. Absorption spectra taken after each experiment indicated that there was no degradation of the samples over the course of the transient absorption runs.

The apparatus for femtosecond transient absorption has been described in detail previously.[48,49] Briefly, a home-built Ti:sapphire regenerative amplifier operating at a 2-kHz repetition rate generates 250-μJ, 130-fs pulses at 828 nm. A portion of this output is split off and focused with all reflective optics through a 3-mm sapphire plate to generate a white-light probe extending from 450 nm through the near-IR region. The remainder of the amplifier output is frequency doubled to generate the 414-nm pump pulse. After passing through the sample, the visible portion of the probe is isolated, dispersed, and detected with a fiber-optic coupled charge-coupled device (CCD, Ocean Optics). Before the sample, the pump is attenuated to 1.0 μJ/pulse, focused to a 200-μm spot within the sample, polarized at 54.7° relative to the probe, and chopped at 50 Hz. Sequential 10-ms pump-on and pump-off exposures of the detector are measured to generate the transient absorption spectrum. The temporal instrument response was measured using the optical Kerr effect (OKE) and was wavelength dependent because of the group-velocity mismatch between the pump and probe wavelengths.[50] OKE cross-correlations ranged from 230 fs at 450 nm to 480 fs at 700 nm. Transient absorption kinetics were fit to a sum of exponentials with a Gaussian instrument function using Levenberg−Marquardt least-squares fitting.

Samples for nanosecond transient absorption spectroscopy were placed in a 10-mm path length quartz cuvette equipped with a vacuum adapter and subjected to five freeze−pump−thaw degassing cycles. The samples were excited with 5-ns, 1-mJ, 420-nm laser pulses generated using the frequency-tripled output of a Continuum 8000 Nd:YAG laser to pump a Continuum Panther OPO. The excitation pulse was focused to a 5-mm diameter spot and matched to the diameter of the probe pulse generated using a xenon flash lamp (EG&G Electrooptics FX-200). The signal was detected using a photomultiplier tube with high voltage applied to only 4 dynodes (Hamamatsu R928). The total instrument response time is 7 ns and is determined primarily by the laser pulse duration. The sample cuvette was placed between the poles of a Walker Scientific HV-4W electromagnet powered by a Walker Magnion HS-735 power supply. The field strength was measured by a Lakeshore 450 gaussmeter with a Hall effect probe. Both the electromagnet and the gaussmeter were interfaced with the data collection computer, allowing measurement and control of the magnetic field to $\pm 1 \times 10^{-5}$ T during data acquisition. Kinetic traces were recorded over a range of 1 μs. Between 50 and 80 shots were averaged at each field strength with a LeCroy 9384 digital oscilloscope and sent to a microcomputer, which calculated the ΔA. Due to the length of the sample runs (>3 h), a small amount of sample degradation was observed, resulting in a decrease in the triplet yield at zero field, $\Delta A(B = 0)$, over the course of the experiments. To compensate for this, the magnetic field was reset to $B = 0$ mT every 3 kinetic traces and $\Delta A(B = 0)$ was plotted and fit with a polynomial or a series of polynomials. These functions were used to calculate the relative triplet yield

as a function of applied field strength. The relative triplet yield is thus

$$\frac{T}{T_0} = \frac{\Delta A(B)}{\Delta A(B=0)}$$

The results presented are an average of two or more experiments conducted on separate days with freshly prepared samples.

Samples for EPR measurements were prepared in toluene (0.2−2 mM), loaded into quartz tubes (4 mm OD × 2 mm ID), and subjected to several freeze−pump−thaw degassing cycles on a vacuum line (10^{-4} mBar). The tubes were then fused with a hydrogen torch and kept in the dark when not being used. The samples were excited at 416-nm, 1-mJ, 7-ns laser pulses from the H_2−Raman shifted output of a frequency-tripled Q-switched Nd:YAG laser (Quanta Ray DCR-2).

Steady-state EPR spectra, transient CW EPR spectra and pulse EPR spectra were measured using a Bruker Elexsys E580 X-band EPR spectrometer with a variable-Q dielectric resonator (Bruker ER 4118X-MS5) at room temperature. Steady-state CW EPR spectra were measured under the conditions of 0.2−2 mW microwave power and 0.01−0.05 mT field modulation at 100 kHz. The g values of the spectra were calibrated with a crystalline 2,2-diphenyl-1-picrylhydrazyl (DPPH) standard (g = 2.0036). Transient CW EPR measurements were carried out under CW microwave irradiation (typically 2−20 mW) by accumulating kinetic traces of transient magnetization following photoexcitation. The field modulation was disabled to achieve a response time $\tau = Q/\pi\upsilon \approx 30$ ns[51] and microwave signals in emission (e) and/or absorption (a) were detected in both the real and the imaginary channels (quadrature detection). Sweeping the magnetic field gave 2D complex spectra vs time and magnetic field. For each kinetic trace, the signal acquired prior to the laser pulse was subtracted from the data. Kinetic traces recorded at off-resonant fields were considered background signals, whose average was subtracted from all kinetic traces. The spectra were subsequently phased into a Lorentzian part and a dispersive part, and the former, also known as the imaginary magnetic susceptibility χ'', is presented.

High-power microwave pulses were generated by a 1-kW TWT amplifier (Applied Systems Engineering 117X). The typical length of a $\pi/2$ pulse was 8 ns. The resonator was fully over-coupled to achieve Q < 200 and a dead time of ~72 ns. All the quadrature-detected spectra were properly phased, and χ'' is presented. In the pulse EPR kinetic measurements, the first microwave pulse was initially timed 200 ns earlier than the laser pulse and was delayed incrementally relative to the laser pulse. A kinetic trace was formed by measuring the intensity of the free induction decay (FID) at different time delays of the microwave pulse with respect to the laser pulse.

Results

Steady-State Properties. The photophysics of the 6ANI chromophore have been previously described in detail.[44,52] Briefly, the electronic absorption spectra of ground-state **1a** and **3a** in toluene have a broad charge-transfer band centered at 397 nm due to 6ANI. The NI acceptor has ground-state absorptions due to $\pi-\pi^*$ transitions at 343, 363, and 382 nm. The PI acceptor and the T• radical have no appreciable ground-state absorption at λ > 350 nm. Steady-state UV−vis spectra of **1b**−**4b**, **5**, and NI in toluene are shown in Figure 1.

The redox potentials for 6ANI, MeOAn, NI, and PI within **1a**−**4a** have been used to calculate the energies of the charge-separated states generated following photoexcitation of 6ANI.[45,53]

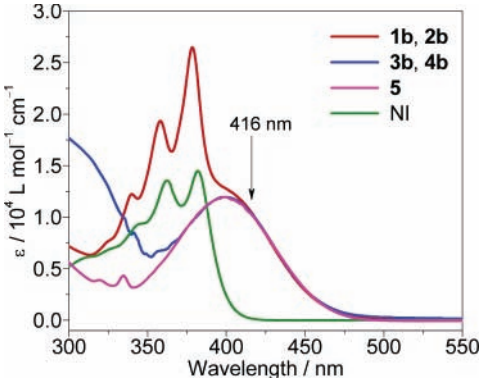

Figure 1. Ground-state UV−vis spectra of the triads **1b**/**2b**, **3b**/**4b**, the dyad **5**, and the NI acceptor in toluene. **1b** and **2b** exhibit essentially the same spectrum and so do **3b** and **4b**. The λ_{max} for PI is 318 nm. T• has very little absorption at λ > 300 nm.

The redox potentials of the corresponding donor and acceptor components within **1b** and **3b** were reported earlier,[41] and those of **2b** and **4b** measured here are unchanged by attachment of T•. Hence, substitution of T• onto the NI or PI acceptors does not change significantly the energetics of CS and CR within **1b**−**4b** relative to those of **1a**−**4a.** Relevant energy level diagrams are given in Figure 2 and numerically in Table S2. The lowest neutral triplet states energies of NI, 6ANI, and PI are 2.03, 2.05, and 2.45 eV, respectively.[41]

Ultrafast Transient Absorption Spectroscopy. Charge separation and recombination time constants for **1a**−**4a** were measured previously and are reported in Table 1.[44,45,54] Charge separation time constants for **1b**−**4b** were determined after direct excitation of 6ANI with 414-nm light by monitoring the femtosecond transient absorption kinetics at λ_{max} of the acceptor radical anions ($NI^{-\bullet}$ at 475 nm in **1b** and 478 nm in **2b**; $PI^{-\bullet}$ at 709 nm in **3b** and 723 nm in **4b**)[53] and at 510−540 nm, where the initial ^{1*}6ANI stimulated emission and subsequent $MeOAn^{+\bullet}$ absorption lie.[44] Representative transient spectra at selected times are shown in Figure 3, while kinetic traces are given in the Supporting Information (Figure S1). In **1b**, the signals at 510 and 475 nm both rise in <0.5 ps, very close to the instrument response of 0.25 ps. However, the transient spectra show no evidence of a broad shoulder between 510 and 540 nm at the earliest positive time delays, indicating that the $NI^{-\bullet}$ species is formed slightly faster than $MeOAn^{+\bullet}$. In contrast, **2b**, which has the dimethylphenyl spacer, shows clear kinetics in which the ^{1*}6ANI stimulated emission is replaced by a distinct $MeOAn^{+\bullet}$ absorption around 500 nm with a time constant of 7 ps. Subsequently, the $NI^{-\bullet}$ signal at 478 nm grows in with a time constant of 400 ps. The kinetics of the PI compounds (**3b** and **4b**) are particularly simple to interpret, because the $PI^{-\bullet}$ absorption is spectrally distinct from the $MeOAn^{+\bullet}$ signal. In **3b**, the ^{1*}6ANI stimulated emission is replaced by $MeOAn^{+\bullet}$ absorption with τ = 2.9 ps, while the appearance of the $PI^{-\bullet}$ signal at 709 nm is dominated by a time constant of 10 ps. In **4b**, the 540-nm kinetics are dominated by the 8-ps growth of the $MeOAn^{+\bullet}$, while the large $PI^{-\bullet}$ peak at 723 nm grows in with τ = 3.5 ns. Thus, in **1a**/**b**, the CS sequence is MeOAn−^{1*}6ANI−NI−X → MeOAn−$6ANI^{+\bullet}$−$NI^{-\bullet}$−X → $MeOAn^{+\bullet}$−6ANI−$NI^{-\bullet}$−X, where X = n-C_8H_{17} or T•, while for triads **2a**/**b**−**4a**/**b** the CS sequence is MeOAn−^{1*}6ANI−Ph_n−A−X → $MeOAn^{+\bullet}$−$6ANI^{-\bullet}$−Ph_n−A−X → $MeOAn^{+\bullet}$−6ANI−Ph_n−$A^{-\bullet}$−X, where A = NI or PI.[45]

Nanosecond Spectroscopy and Magnetic Field Effect Measurements. We have reported that attaching T• to NI increases the RP lifetime of **1b** (τ = 49.9 ns) to almost twice

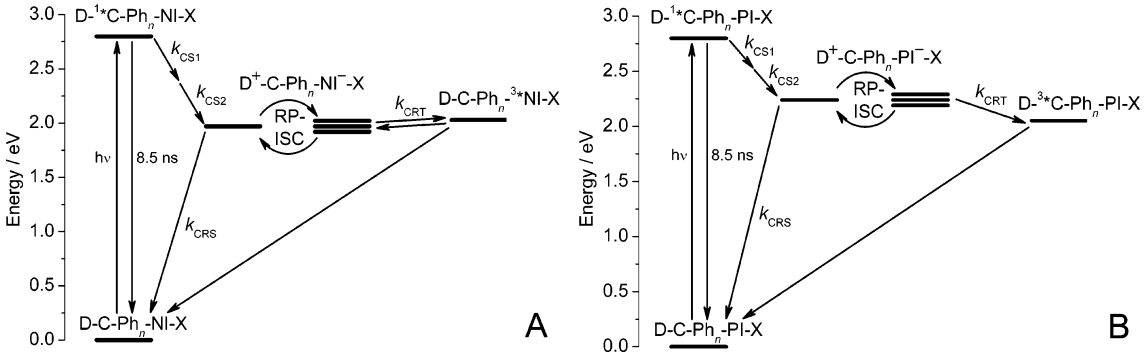

Figure 2. Electron-transfer pathways: (A) **1a/b** and **2a/b** and (B) **3a/b** and **4a/b,** where D = MeOAn, C = 6ANI, X = *n*-C_8H_{17} or T•, and *n* = 0 or 1. The Zeeman splittings of the RP triplet states are exaggerated by a factor of 10^4.

TABLE 1: Time Constants for CS and CR and Magnitudes of 2*J* Determined by MFE in Toluene

compound	τ_{CS1} (ps)	τ_{CS2} (ps)	τ_{CR} (ns)	2*J* (mT)
1a	0.7 ± 0.2	1.3 ± 0.5	28.5 ± 0.5	47.5 ± 0.5
1b	<0.5	<1.0	49.9 ± 0.5	47.0 ± 0.5
2a	9.8 ± 0.2	430 ± 20	210 ± 5	1 ± 0.5
2b	7.0 ± 0.2	400 ± 20	506 ± 10	<1
3a	2.7 ± 0.2	19 ± 5	18.0 ± 0.5	66 ± 0.5
3b	2.9 ± 0.2	10 ± 3	10.5 ± 0.5	60 ± 0.5
4a	6.9 ± 0.2	5000 ± 500	73 ± 2	2, 19 ± 0.5
4b	8.0 ± 0.2	3500 ± 500	109 ± 3	1, 16 ± 0.5

as long as that of **1a** (τ = 28.5 ns).[41] A similar increase in RP lifetime is observed for **2b** (τ = 506 ns) relative to **2a** (τ = 210 ns) and for **4b** (τ = 109 ns) relative to **4a** (τ = 73 ns). Conversely, the RP lifetime of **3b** (T = 10.5 ns) is about 40% shorter than that of **3a** (τ = 18 ns).

Magnetic field effects (MFEs) on the yield of the lowest neutral triplet states that result from RP-ISC followed by CR reveal the exchange coupling 2*J* between the radical ions within the pair; see Table 1.[55,56] The MFEs for **2b** and **4b** are shown in Figure 4, while those for the remaining molecules have been reported earlier.[41,45] Two values for 2*J* are observed for **4a** and **4b** that most likely result from two slightly different conformations that lead to differences in the electronic coupling between the radicals.[57] The MFE experiment demonstrates little difference between the values of 2*J* measured in the presence and absence of T• for a given triad, where 2*J* = 1.0 mT and <1.0 mT for **2a** and **2b**, respectively, while 2*J* = 2 mT, 19 mT, and 1 mT, 16 mT for **4a** and **4b**, respectively. As expected, the shorter triads have much larger exchange couplings, with the 2*J* resonances for **1a** and **1b** occurring at 47.5 and 47.0 mT, respectively, and those for **3a** and **3b** occurring at 66 and 60 mT, respectively. Thus, attachment of T• does not significantly change the energy gap between RP_S and RP_T in all pairs of molecules.

EPR Spectroscopy. Each T•-containing triad, **1b**−**4b,** has a doublet ground state (D_0) with the total spin density tightly confined to the N−O bond of T• by its aliphatic backbone. This is confirmed by the CW EPR spectra of **1b**−**4b,** which exhibit the three-line hyperfine splitting characteristic of T•, with $|a_N|$ = 1.54 mT and g = 2.0057. A representative spectrum for **2b** is shown in Figure 5. In contrast to the unsubstituted T• radical, the line widths of the three hyperfine lines are nonlinearly dependent on the nuclear quantum number *M*. On the other hand, the small splittings caused by the 12 methyl protons with $|a_H|$ = 0.040 mT are resolved, and line shape simulations with WinSim[58] reveal the homogeneous line broadening to be ≤0.026 mT, equivalent to a T_2 of ≥0.4 μs. Both the hyperfine-dependent line widths and the prolonged relaxation time signify relatively

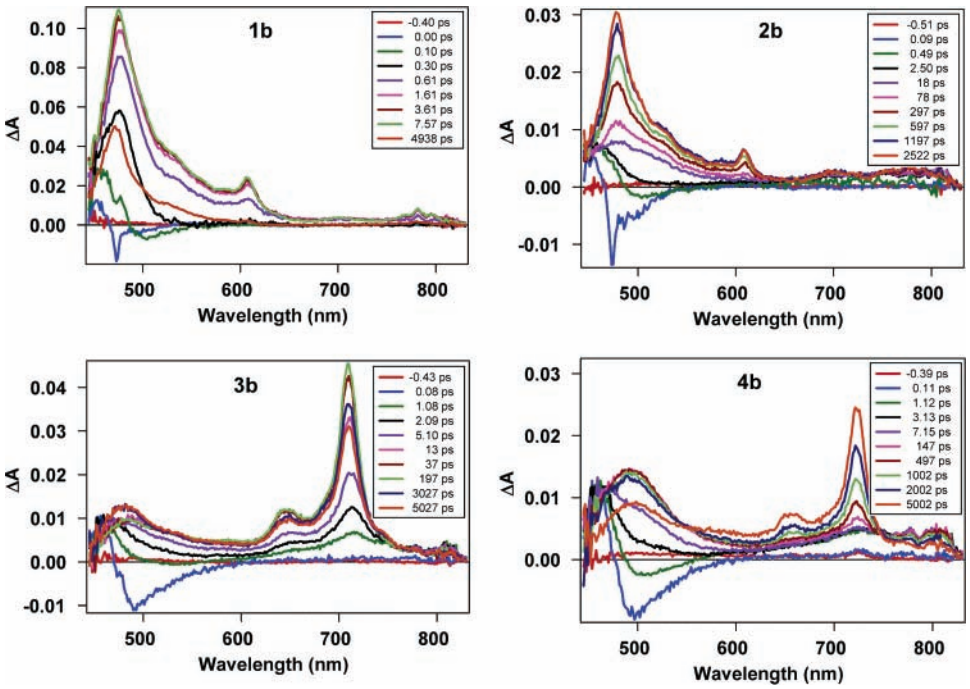

Figure 3. Femtosecond transient absorption spectra of **1b** (MeOAn−6ANI−NI−T•), **2b** (MeOAn−6ANI−Ph−NI−T•), **3b** (MeOAn−6ANI−PI−T•), and **4b** (MeOAn−6ANI−Ph−PI−T•) in toluene following excitation by a 414-nm 130-fs laser pulse.

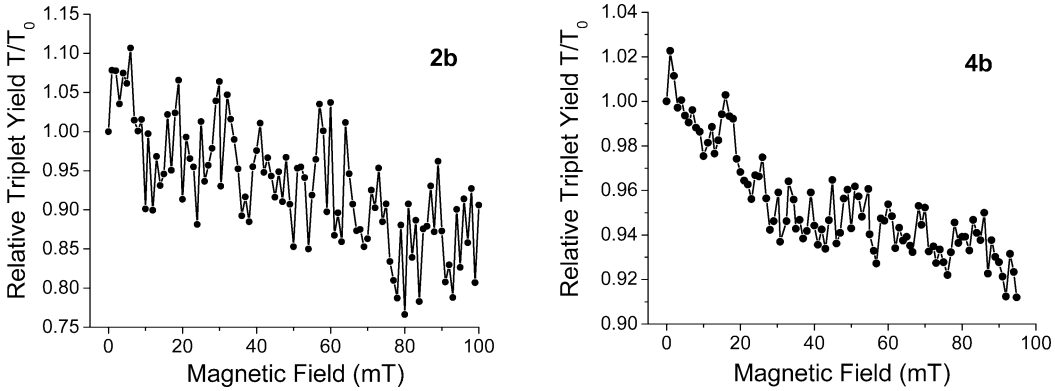

Figure 4. Magnetic field effects on the triplet yield of the indicated molecules in toluene.

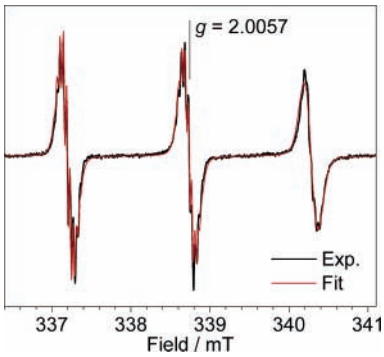

Figure 5. Steady-state CW EPR spectrum, in the derivative form, of $\sim 10^{-4}$ M **2b** in toluene. EPR spectra of other triads **1b**, **3b**, and **4b** are similar. The black curve is the experiment result, and the red curve is the simulation, which yields $g = 2.0057$, $|a_N| = 1.54$ mT, and $|a_H| = 0.040$ mT ($\times$ 12).

slow rotational averaging of the g and hyperfine anisotropies,[59,60] which can be attributed to the covalent attachment of T$^{\bullet}$ to the relatively large triad systems.

At room temperature in toluene, molecular tumbling renders EPR spectra of molecular triplet states broad and structureless,[61] if not completely undetectable. Thus, time-resolved EPR spectra observed around $g \approx 2.00$, Figure 6, are due to both the photogenerated RPs and the neutral T$^{\bullet}$ radicals. Immediately after laser excitation, the **2b** and **4b** triads show an intense signal with an emission, absorption (*e*,*a*) polarization pattern, centered at $g = 2.0033$ (**2b**) or 2.0035 (**4b**), very close to the g values of MeOAn$^{+\bullet}$ and the respective NI$^{-\bullet}$ or PI$^{-\bullet}$ radical ions,[57,62] which is assigned to the photogenerated RP state. For all four triads **1b**−**4b,** a new set of emissive peaks grow in at long times, which have identical g factors, hyperfine splittings, and line widths to those measured in the dark, Figure 5, and are thus

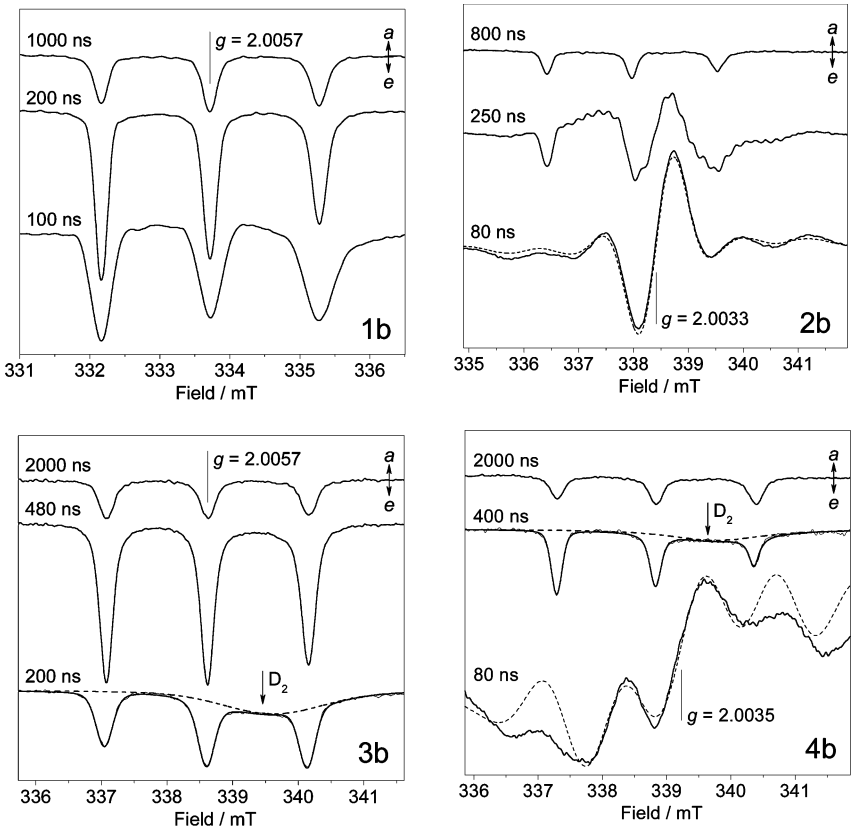

Figure 6. Transient CW EPR spectra of the RP state and/or the polarized T$^{\bullet}$ of **1b, 2b, 3b**, and **4b**, at various times after the laser pulse, in toluene at room temperature. Dashed lines are fitted line shapes of the RP and D_2 states (see text). **3b** and **4b** show a broad and relatively weak signal in emission centered at $g \sim 2.000$ superimposed on the T$^{\bullet}$ peaks; this signal is designated as the D_2 state (see text).

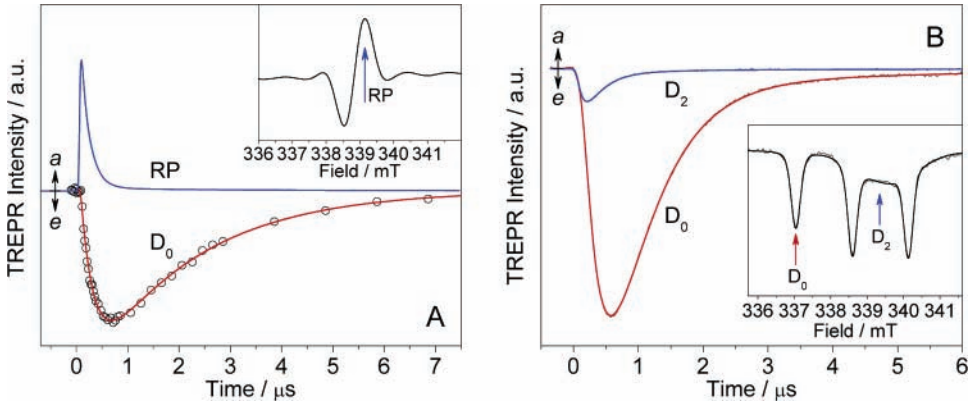

Figure 7. (A) Blue curve: transient CW kinetic trace of **2b** after laser excitation ($t = 0$); red curve: FID-detected kinetic trace of the polarized D_0 (see text). (B) Transient CW kinetic traces of the polarized D_0 (red) and D_2 (blue) states of **3b**. All three transient CW traces are measured at the fields indicated in the respective inset: (A) 338.7 mT, (B) 337.1 mT for the D_0 state, and 339.4 mT for D_2.

signals from the T• moiety, which becomes transiently polarized following charge recombination of the RP state.

The TREPR kinetics of the RP and the polarized T• in the ground state (labeled D_0) are shown for **2b** and **3b** in Figure 7. These kinetic traces are measured at the field values indicated in the insets, where signals from different states are reasonably well separated. For **2b**, where the RP signal is broad and very intense, the kinetic behavior of the transient polarization at T• is monitored using the magnitude of its free induction decay (FID) at various times with pulse EPR, taking advantage of the good temporal fidelity of the pulse technique at long times over transient CWs methods.[63] More importantly, in contrast to doublet radicals, the FID signals from spin-correlated RPs are suppressed by a $\pi/2$ microwave pulse[64−66] and thus do not interfere with selective observation of the polarized T•. The kinetic traces for **2b** and **3b** are fit well with a rise−decay biexponential model. For **2b**, the decay of the RP signal ($\tau = 169 \pm 1$ ns) occurs faster than the emergence ($\tau = 252 \pm 9$ ns) of the polarized T•; see Figure 7A. The RP signal lifetime measured by TREPR reflects polarization decay and differs from the intrinsic lifetime of the RP state measured by transient absorption; see Table 1. In the case of **3b**, the RP state decays too fast ($\tau_{CR} = 10.5$ ns by transient absorption) to observe by TREPR. The polarization decay time of T• ($\tau = 1.83 \pm 0.04$ for **1b** and 2.07 ± 0.06 μs for **2b**) conforms to the usual spin−lattice relaxation time T_1 of nitroxides at room temperature.[67]

At early times, the TREPR spectra of **3b** and **4b** exhibit a broad, emissive peak growing in at a low g value of 2.000 ± 0.001; see Figure 6. This signal is assigned to the recombinant states ^{2}(MeOAn−^{3*}6ANI−$Ph_{0,1}$−PI−T•), labeled D_2 (see Discussion). In X- and W-band TREPR studies[68,69] of zinc tetraphenylporphyrin (ZnTPP) coordinated to a pyridyl nitronyl nitroxide (nitpy) free radical, the g value of its excited doublet state, ^{2}(^{3*}ZnTPP−nitpy•), was determined to be 2.0016 ± 0.0002, even though its ground state has a g value as high as 2.0068 ± 0.0002. From Figures 6 and 7, the D_2 state of **3b** and **4b** exhibits very broad peaks relative to those of D_0, while in **1b** and **2b**, the D_2 signal is overwhelmed by the intense D_0 or RP polarization. This is most likely due to lifetime-broadening of the transient D_2 state. In terms of lifetimes, Figure 7B, the D_2 decay time of **3b** ($\tau_1 = 283 \pm 6$ ns) matches the D_0 rise time ($\tau_2 = 285 \pm 2$ ns) very well. These kinetic data are consistent with the polarized D_0 ground state being generated via the CR pathway RP → D_2 → D_0 (see Discussion). The kinetics of the different states of **4b** following photoexcitation are severely convoluted with one another, preventing an unequivocal analysis.

Discussion

Energetics and Electron-Transfer Dynamics. The CS time constants given in Table 1 show that the rates of the CS reactions for the series of molecules with T• (**1b**−**4b**) are similar to those without T• (**1a**−**4a**). This is reasonable and expected given that these CS rates are much faster than RP-ISC and thus should not be influenced by the presence of the third spin.[70−75] In contrast, the T• radical clearly influences the slower CR dynamics, as evidenced by the different CR time constants exhibited by the T•− and octyl-terminated molecules. The energy levels and charge-transfer pathways shown in Figure 2 provide a basis for explaining these effects, while the detailed spin dynamics will be discussed in sections below. The total reorganization energy (λ_{CR}) for CR in **1a/b**−**4a/b** is 0.54−0.79 eV (see Table S2), so that the CR of the final RP product to the singlet ground state (k_{CRS}) lies deep within the Marcus inverted region[76] for each of these triads and hence is relatively slow. Charge recombination of the RP to the lowest neutral triplet state (k_{CRT}) lies in the Marcus normal region and depends strongly on the free energy for this process, so that the relative magnitudes of k_{CRS} and k_{CRT} as well as the relative populations of RP_S and RP_T determine the overall measured CR rate. RP-ISC between RP_S and RP_T usually occurs slowly via the hyperfine mechanism; however, the paramagnetic T• radical creates a strong local magnetic field that accelerates RP-ISC resulting in rapid population of RP_T. This mechanism has been termed spin catalysis or enhanced intersystem crossing (EISC).[32,34,39,77]

Photoinitiated two-step CS within **1b**−**4b** rapidly produces triradicals, ^{2}(MeOAn^{+}•−6ANI−Ph_n−A−•−T•), where A = NI or PI and $n = 0$ or 1, having overall doublet spin configurations. Charge recombination within ^{2}(MeOAn^{+}•−6ANI−Ph_n−A−•−T•) produces the doublet ground state ^{2}(MeOAn−6ANI−Ph_n−A−T•) (k_{CRS}), Figure 2, while EISC leads to a triradical having a pair of doublet states and a quartet state: ^{2,4}(MeOAn^{+}•−6ANI−Ph_n−A−•−T•). Depending on whether A = NI or PI, CR within the triradical (k_{CRT}) produces the neutral doublet and quartet states ^{2,4}(MeOAn−6ANI−Ph_n−^{3*}NI−T•) or ^{2,4}(MeOAn−^{3*}6ANI−Ph_n−PI−T•), respectively.[46,78] Note that in this case two unpaired electrons reside on ^{3*}NI or ^{3*}6ANI, so that these species are formally "triplet" excited states that can be observed optically.

The free energy of the CR process ^{2,4}(MeOAn^{+}•−6ANI−Ph_n−NI−•−T•) → ^{2,4}(MeOAn−6ANI−Ph_n−^{3*}NI−T•) in **1a/b** and **2a/b** is 0.06 eV, so that an equilibrium between these states is established.[46] In contrast, for the corresponding CR process

^{2,4}(MeOAn$^{+\bullet}$−6ANI−Ph$_n$−PI$^{-\bullet}$−T$^{\bullet}$) → ^{2,4}(MeOAn−^{3*}6ANI−Ph$_n$−PI−T$^{\bullet}$) in **3a/b** and **4a/b,** $\Delta G = -0.2$ eV, so that k_{CRT} is faster than that for **1a/b** and **2a/b** and there is no equilibrium.[79]

The lifetime of triradical ^{2,4}(MeOAn$^{+\bullet}$−6ANI−NI$^{-\bullet}$−T$^{\bullet}$) in **1b** ($\tau_{CR} = 49.9$ ns) is almost double that of the corresponding RP in **1a** ($\tau_{CR} = 28.5$ ns). Similarly, the lifetime of triradical ^{2,4}(MeOAn$^{+\bullet}$−6ANI−Ph−NI$^{-\bullet}$−T$^{\bullet}$) in **2b** ($\tau_{CR} = 506$ ns) is more than double that of the corresponding RP in **2a** ($\tau_{CR} = 210$ ns). Given that the triradicals in **1b/2b** and the RPs in **1a/2a** are in equilibrium with their respective ^{2,4}(MeOAn−6ANI−Ph$_n$−^{3*}NI−T$^{\bullet}$) states,[78] EISC driven by the presence of T$^{\bullet}$ in **1b/2b** shifts the population toward the corresponding RP$_T$, which presents a bottleneck to overall CR decay due to the fact that ^{2,4}(MeOAn−6ANI−Ph$_n$−^{3*}NI−T$^{\bullet}$) is slightly higher in energy than ^{2,4}(MeOAn$^{+\bullet}$−6ANI−Ph$_n$−NI$^{-\bullet}$−T$^{\bullet}$).

In contrast, the lifetime of triradical ^{2,4}(MeOAn$^{+\bullet}$−6ANI−PI$^{-\bullet}$−T$^{\bullet}$) in **3b** ($\tau_{CR} = 10.5$ ns) is about a factor of 2 shorter than **3a** ($\tau_{CR} = 18$ ns), and the yield of CR product ^{2,4}(MeOAn−6ANI−^{3*}PI-T$^{\bullet}$) increases significantly upon addition of the T$^{\bullet}$ radical.[41] As noted above, based on energetic considerations, k_{CRT} should be much larger than k_{CRS} for **3a/b**. EISC increases the rate at which RP$_T$ is produced, so that a larger RP population accesses the more efficient triplet recombination pathway leading to both an increased CR rate and yield of ^{2,4}(MeOAn−6ANI−^{3*}PI−T$^{\bullet}$). Given the similar energetics of **3a**/**b** and **4a**/**b**, we would expect the same relative ordering of CR rates for **4a/b** as were observed for **3a/b**. However, the lifetime of triradical ^{2,4}(MeOAn$^{+\bullet}$−6ANI−Ph-PI$^{-\bullet}$−T$^{\bullet}$) in **4b** ($\tau_{CR} = 109$ ns) is about 50% longer than that of **4a** ($\tau_{CR} = 73$ ns). This divergence between **3b** and **4b** is most likely due to the fact that the CR rate is determined by factors other than simply the free energy change. We have shown recently in a variant-temperature study that in **1a** the electronic coupling for charge recombination between MeOAn$^{+\bullet}$ and NI$^{-\bullet}$ is gated by conformational motions within the molecule and k_{CRT} exceeds k_{CRS} only at temperatures above 280 K.[80]

Electron Spin−Spin Couplings in the Photogenerated Triradical. It was shown years ago[81] that the value of 2J in biradical **6** involving nine σ bonds and two π bonds between the two nitroxide radicals greatly exceeds the 1.44 mT hyperfine coupling of these radicals.

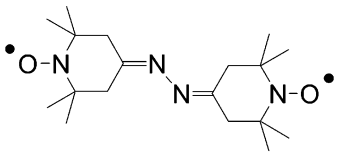

6

Also, Mori et al.[37] studied the NI$^{-\bullet}$−T$^{\bullet}$ biradical anion with a spin−spin distance of 8.44 Å in the steady state and estimated $2J \approx 1$ T (10^{-4} eV). Therefore, we can assume that the exchange coupling between PI$^{-\bullet}$ and T$^{\bullet}$ over a slightly shorter distance (center-to-center 8.2 Å[82]) will be comparable or even larger, because of the similarity between the structures of NI and PI. Our previous research on the **1a**−**4a** control dyads, including MFE[45,54,55] and TREPR[57] experiments, has shown that the exchange coupling within the RP is on the order of tens of millitesla for MeOAn$^{+\bullet}$−6ANI−A$^{-\bullet}$ and 1−2 mT for MeOAn$^{+\bullet}$−6ANI−Ph−A$^{-\bullet}$, where A = NI or PI, as listed in Table 1. Last, the exchange coupling between MeOAn$^{+\bullet}$ and T$^{\bullet}$ must be negligibly weak, since they lie at the two termini of all the rodlike triads and 2J decays exponentially as a function of spin−spin distance.[75]

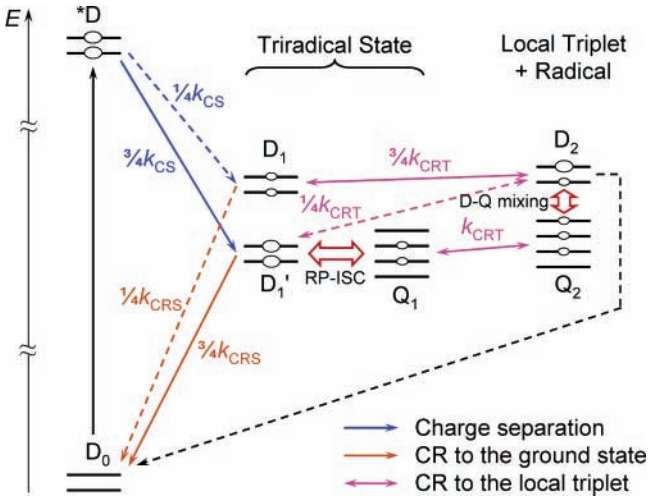

Figure 8. Energy level diagram showing the spin manifolds of **1b**−**4b** after charge separation and charge recombination, in a magnetic field of ~0.35 T. Blue arrows denote charge separation forming the triradical state; orange arrows, charge recombination to the ground doublet state; and magenta arrows, reversible D−D and Q−Q charge recombination steps leading to the local triplet ^{3*}NI, which is nearly isoenergetic with the RP state in toluene (see text). D_1, D_1', and Q_1 form a complete spin basis set of the triradical state. Dashed lines mean less probable transitions. Red double arrows stand for processes that mix certain Zeeman levels of the relevant D and Q states. The size of the ellipse on each spin level represents its population qualitatively.

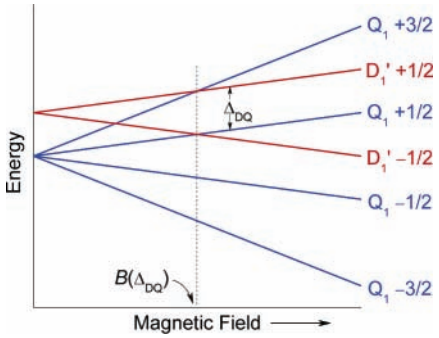

Figure 9. Zeeman splitting of the D_1' and Q_1 states as a function of the magnetic field. There are two level crossings at the field strength equivalent to Δ_{DQ}, at which the MFE resonance appears.

Following photoexcitation, the triradical MeOAn$^{+\bullet}$−6ANI−Ph$_n$−A$^{-\bullet}$−T$^{\bullet}$ has three pairs of exchange interactions, $2J_{DA}$, $2J_{DT}$, and $2J_{AT}$, where the subscripts denote the spins on MeOAn$^{+\bullet}$, A$^{-\bullet}$, and T$^{\bullet}$, respectively, and $2J_{AT}$ dominates, following the above analysis for the individual two-spin subsystems. These noncommutative exchange interactions remix the spin manifold into two doublets and a quartet,[32] shown in Figure 8 as D_1, D_1', and Q_1 states. As usual, Q_1 refers to the state where all the three spins are parallel, and in the two doublet states, only one pair of them is parallel. Here, we use D_1' to label the state in which the parallel pair of spins lies on A$^{-\bullet}$ and T$^{\bullet}$. We use D_1 to label the other doublet state (see Appendix for their wave functions). Now that D_1' and Q_1 both possess parallel A$^{-\bullet}$ and T$^{\bullet}$ spins, their energy levels are close to each other, but far removed from D_1, due to the magnitude of $2J_{AT}$. On the other hand, the small energy gap between D_1' and Q_1 at zero field, denoted Δ_{DQ} in this paper, can be calculated as a complicated expression in terms of all three pairs of 2J values[32] and turns out to be comparable with the small values of $2J_{DA}$ and $2J_{DT}$.

In Figure 9, we plot the Zeeman splittings of D_1' and Q_1 as a function of the external magnetic field. It is clear that, at the

field strength equivalent to Δ_{DQ}, the two Zeeman sublevels $|D_1' + 1/2\rangle$ and $|Q_1 + 3/2\rangle$ cross each other and so do $|D_1' - 1/2\rangle$ and $|Q_1 + 1/2\rangle$. This means that at the level-crossing point $B(\Delta_{DQ})$, the rate of RP-ISC from D_1' to Q_1, driven by nuclear spin flips, is maximized, and a peak in local triplet yield appears in the MFE plot. However, the transition $|D_1' - 1/2\rangle \rightarrow |Q_1 + 3/2\rangle$ is still a forbidden process even though they coincide at $1/2B(\Delta_{DQ})$. On the other hand, in the EPR context where the high-field limit is appropriate, only those Zeeman sublevels with the same m_S number, namely, $|D_1' \pm 1/2\rangle$ and $|Q_1 \pm 1/2\rangle$, are subject to hyperfine mixing. In other words, the well-known $S-T_0$ mixing mechanism[47,55,63,83] of RP-ISC directly translates into $D \pm 1/2 - Q \pm 1/2$ mixing in this context and TREPR spectra with the same polarization pattern should be observed. This is a consequence of the fact that the two Zeeman sublevels of D_1' are split by only ~0.35 T or $\sim 10^{-5}$ eV, which is negligible compared with the overall free energy change for charge separation $\Delta G(^*D \rightarrow D_1') \cong -0.8$ eV (**1b**/**2b**) or −0.5 eV (**3b**/**4b**), Figure 2, producing a nonpolarized D_1' state (ignoring thermal polarization), which is analogous to the singlet RP produced in the **1a**−**4a** model systems. The Q_1 state is not populated initially as a result of spin conservation during the ultrafast charge separation. The D_1 state, which is energetically far removed from the D_1' and Q_1 states, does not mix with them at ~0.35 T, the field strength at which all TREPR spectra were measured.

The above reasoning is corroborated by the TREPR and MFE results for **1b**−**4b**, which both probe the $D_1'-Q_1$ splitting, Δ_{DQ}, of the triradical RP state.[41] The TREPR spectra of MeOAn$^{+\bullet}$−6ANI−Ph−NI$^{-\bullet}$−T$^\bullet$ and MeOAn$^{+\bullet}$−6ANI−Ph−PI$^{-\bullet}$−T$^\bullet$, Figure 6, are simulated with a two-state-mixing model similar to the one outlined previously,[57] yielding $\Delta_{DQ} = 0.65$ mT and 1.8 mT, respectively, in agreement with the values obtained with MFE. In this model, the $|D_1' \pm 1/2\rangle$ and $|Q_1 \pm 1/2\rangle$ states are mixed by ΔB, the difference in local magnetic environments of the individual spins due to hyperfine interactions and spin−orbit coupling. This makes all four transitions from $|D_1' + 1/2\rangle$ or $|Q_1 + 1/2\rangle$ partially allowed, two toward $|Q_1 + 3/2\rangle$ in absorption (*a*) and the other two toward $|Q_1 - 1/2\rangle$ in emission (*e*) and likewise in the case of $|D_1' - 1/2\rangle$ or $|Q_1 - 1/2\rangle$. The overall observed TREPR spectra are simulated by the sum of all the above *e* and *a* peaks weighted by the nuclear spin states, and the RP sign rule[47,57] indicates the sign of Δ_{DQ} from the polarization pattern of field-swept TREPR spectra

$$\Gamma = \mu \cdot \mathrm{sign}(\Delta_{DQ}) = \begin{cases} -ea \\ +ae \end{cases} \tag{1}$$

where μ equals −1 or +1 for a doublet or a quartet precursor, the former being the case here. Therefore, the experimental *e a* pattern confirms Δ_{DQ} to be positive, that is, D_1' is higher in energy than Q_1. Compared with the S−T splittings in the RP states of the **2a** and **4a** dyads (Table 1), the $D_1'-Q_1$ splittings of **2b** and **4b** decrease slightly when T$^\bullet$ is introduced. The TREPR spectra of MeOAn$^{+\bullet}$−6ANI−NI$^{-\bullet}$−T$^\bullet$ (the RP state of **1b**) and MeOAn$^{+\bullet}$−6ANI−PI$^{-\bullet}$−T$^\bullet$ (that of **3b**) are not observed, as well as their parent molecules **1a** and **3a**, partly because of their fast CR rate (τ_{CR} = 49.9 and 10.5 ns, respectively) and partly because of the low EPR line intensities determined by[63]

$$I \propto \Delta B^2/(\Delta_{DQ}{}^2 + \Delta B^2) \tag{2}$$

where ΔB ranges between −3.0 and 3.0 mT, compared with Δ_{DQ} of **1b** and **3b** measured to be 47 and 60 mT, respectively see Table 1. Nonetheless, the existence of the RP state in these systems has been verified by the ultrafast transient absorption results shown earlier in this paper.

Charge Recombination and Switching the Spin Basis Set. Our earlier studies of **1a**−**4a**,[44,45,54] **1b**, and **3b**,[41] as well as other closely related molecules,[55,57,78] have shown that RP-ISC is followed by CR, returning part of the population to the ground-state D_0 and the remainder to the states MeOAn−6ANI−Ph$_n$−^{3*}NI−T$^\bullet$ or MeOAn−^{3*}6ANI−Ph$_n$−PI−T$^\bullet$. The neutral free radical T$^\bullet$ is spin coupled to NI$^{-\bullet}$ or PI$^{-\bullet}$ with $2J_{AT} \approx 10^{-4}$ eV, and therefore does not redirect the charge recombination, but instead establishes a new basis set of doublet and quartet states, labeled in Figure 8 as D_2 and Q_2. No spin flip occurs during charge recombination, so that the Q_2 state inherits the population of the ±1/2 sublevels of Q_1 generated by RP-ISC from D_1'. However, the D_2 state becomes a mixture of the D_1' and D_1 states,[84] because CR is accompanied by the rise of an extremely large same-site exchange interaction between the two unpaired spins of ^{3*}NI or ^{3*}6ANI, which are estimated at 0.90 and 0.75 eV, their respective S_1-T_1 gap.[78] Thus, D_0, D_2, and Q_2 form a complete spin basis set for the recombinant states, which are different from the other set, D_1, D_1', and Q_1, which characterizes the three-spin RP state.

Consequently, CR from the RP state requires switching or projection of the spin basis set. Generally speaking, CR rates depend explicitly on the electronic coupling *V*

$$k_{CR} = (2\pi/h)\langle \Psi_f|V|\Psi_i\rangle^2 \,(\mathrm{FCWD}) \tag{3}$$

where FCWD is the Franck−Condon weighted density of states[85] and $\Psi_k = \psi_k S_k$ (k = i, f) are the wave functions of the initial and final states, including their orbital (ψ) and spin (S) components. The electronic coupling *V* operates only on the orbital wave function so that eq 3 can be expanded to give

$$k_{CR} = (2\pi/h)\langle \psi_f|V|\psi_i\rangle^2\langle S_f|S_i\rangle^2 \,(\mathrm{FCWD}) \tag{4}$$

Upon photoexcitation, the **1a**−**4a** model triads form biradicals with one singlet sublevel ^{1}(MeOAn$^{+\bullet}$−6ANI−Ph$_n$−A$^{-\bullet}$) and three triplet sublevels ^{3}(MeOAn$^{+\bullet}$−6ANI−Ph$_n$−A$^{-\bullet}$), which subsequently recombine, respectively, to the singlet ground-state MeOAn−6ANI−Ph$_n$−A and the lowest triplet state MeOAn−6ANI−Ph$_n$−^{3*}NI or MeOAn−^{3*}6ANI−Ph$_n$−PI with the singlet and triplet CR rates

$$k_{CRS} = (2\pi/h)\langle \psi_S|V|\psi_{RP}\rangle^2 \,(\mathrm{FCWD})_S \tag{5a}$$

and

$$k_{CRT} = (2\pi/h)\langle \psi_T|V|\psi_{RP}\rangle^2 \,(\mathrm{FCWD})_T \tag{5b}$$

where the spin projections are dropped, since both recombination processes conserve the spin wave function to the zeroth order. The presence of the third spin on T$^\bullet$ has negligible effects on the orbital wave functions ψ_S, ψ_T, and ψ_{RP} or on the $(\mathrm{FCWD})_{S,T}$. Rather, it reshapes the spin subspace such that the spin projections $\langle S_f|S_i\rangle^2$ become (see Appendix)

$$\langle D_0|D_1'\rangle^2 = \langle D_2|D_1\rangle^2 = 3/4 \tag{6a}$$

$$\langle D_2|D_1'\rangle^2 = \langle D_0|D_1\rangle^2 = 1/4 \tag{6b}$$

$$\langle Q_2|Q_1\rangle^2 = 1 \tag{6c}$$

Plugging eqs 6a−6c back into eq 4 yields the CR rates from the three-spin state MeOAn$^{+\bullet}$−6ANI−Ph$_n$−A$^{-\bullet}$−T$^\bullet$ in terms

of k_{CRS} and k_{CRT} as shown in Figure 8. In the following, we continue to use k_{CRS} and k_{CRT}, defined in eq 5, in the context of doublets and quartets so as to compare the charge recombination rates of **1a**−**4a** and **1b**−**4b** conveniently. Note that eq 6c implies that the rate of CR from the quartet triradical state Q_1 is the same as if the third spin does not exist: $k_{CR}(Q_1 \rightarrow Q_2) = k_{CRT}$. In contrast, the total observed k_{CR} from the D_1' state turns into a weighted average of k_{CRS} and k_{CRT}

$$k_{CR}(D_1' \rightarrow D_0 + D_2) \approx 3/4\, k_{CRS} + 1/4\, k_{CRT} \qquad (7)$$

compared with k_{CRS} for the singlet RP state ^{1}(MeOAn$^{+\bullet}$−6ANI−Ph$_n$−A$^{-\bullet}$) of the **1a**−**4a** model triads. This recombination rate is similar for the D_1 state and also qualitatively correct if an effective overall decay rate out of both D_1 and D_1' states is considered. Accordingly, overall CR from the triradical state is accelerated if $k_{CRT} > k_{CRS}$ and otherwise slowed down. In the cases of **1a** and **2a**, where MeOAn$^{+\bullet}$−6ANI−Ph$_n$−NI$^{-\bullet}$ is in equilibrium with MeOAn−6ANI−Ph$_n$−^{3*}NI, it has been shown that the net $k_{CRT} < k_{CRS}$,[80,86] and thus MeOAn$^{+\bullet}$−6ANI−Ph$_n$−NI$^{-\bullet}$−T$^{\bullet}$, lives longer by coupling to the third spin (50 ns vs 28 ns for **1a**/**b** and 506 ns vs 210 ns for **2a**/**b**, Table 1), as observed here by both nanosecond transient absorption and TREPR. The situation is reversed for MeOAn$^{+\bullet}$−6ANI−PI$^{-\bullet}$, where k_{CRS} lies deeply in the Marcus inverted region while k_{CRT} is basically barrierless,[86] namely, $k_{CRT} > k_{CRS}$, so that in **3b** the RP lifetime decreases from 18 to 10.5 ns. Finally, the experimental observations that MeOAn$^{+\bullet}$−6ANI−Ph−PI$^{-\bullet}$−T$^{\bullet}$ has a longer lifetime than MeOAn$^{+\bullet}$−6ANI−Ph−PI$^{-\bullet}$ suggests that like **1a/b** and **2a/b** $k_{CRT} < k_{CRS}$ in these two photogenerated species. One structural property that distinguishes **4a**/**b** from all the other molecules examined here is that the single bond between the 2,5-dimethylphenyl spacer (Ph) and the five-membered cyclic imide of PI has the least amount of steric hindrance to torsional motion. Increased torsional motion increases the $\pi-\pi$ interaction between Ph and PI leading to an increase in V_{DA}, the electronic coupling matrix element between MeOAn$^{+\bullet}$ and PI$^{-\bullet}$. At room temperature, torsional motion around this bond most likely modulates k_{CRS} and k_{CRT} to differing degrees, which may once again lead to $k_{CRT} < k_{CRS}$.

Spin Polarization following Charge Recombination. The observed polarization of T$^{\bullet}$ following CR is unusual, Figures 6 and 7, since the CS, CR, and RP-ISC processes in these systems do not generate a net overall spin polarization. The theory of chemically induced dynamic electron polarization[87] (CIDEP) has been well established for doublet−doublet[63,83,88] and triplet−doublet[89−92] interactions, when these paramagnetic species diffuse in solution. We have examined **2b** at concentrations ranging from 0.2 to 2 mM and find no appreciable difference in the spectra or kinetics. It is also conceivable that *intramolecular* spin−spin interactions occur at rates orders of magnitudes faster than *intermolecular* processes. The overall spin polarization in the system can be traced back to nonadiabatic spin evolution driven by hyperfine interactions, spin−orbit coupling, and/or zero-field splitting (ZFS). Moreover, Gast and Hoff[71,93,94] observed that reduction of the ubiquinone electron acceptor (UQ) in the primary electron transport cofactor sequence of bacterial photosynthetic reaction center proteins, (BChl)$_2$−BPheo−UQ$^{-\bullet}$, followed by photogeneration of the primary radical pair, (BChl)$_2^{+\bullet}$−BPheo$^{-\bullet}$−UQ$^{-\bullet}$, results in a net emissively polarized UQ$^{-\bullet}$, which they attributed to polarization transfer from the nearby BPheo$^{-\bullet}$ due to spin−spin exchange coupling of BPheo$^{-\bullet}$ with UQ$^{-\bullet}$.

A variety of triplet-radical systems have been studied, in which T$^{\bullet}$ is attached, covalently or as a ligand, to molecules such as C_{60},[60,95] porphyrins,[61,68,69] and phthalocyanines.[40] Upon photoexcitation, these large conjugate π systems undergo spin−orbit intersystem crossing (SO-ISC) to form polarized doublet and quartet states, as opposed to the electron-transfer and RP-ISC processes in our D−C−A triads. The presence of the electron-transfer pathway makes it necessary to introduce a new spin basis set, that is, D_1, D_1', and Q_1, to describe the charge-separated triradical states, in addition to the existing set *D, D_2, and Q_2, which have been established for the neutral excited states in systems for which SO-ISC occurs.[61,92,96] A second noteworthy difference is that in the above-mentioned triplet-radical systems the three spin−spin distances are better balanced than those in MeOAn−6ANI−Ph$_n$−^{3*}NI−T$^{\bullet}$ or MeOAn−^{3*}-6ANI−Ph$_n$−PI−T$^{\bullet}$. Accordingly, the three unpaired spins in the delocalized triplet-radical systems experience similar pairwise exchange and dipolar interactions and as a whole behave more like an ideal quartet. On the other hand, the difference between the magnetic environments of the local triplet (^{3*}NI or ^{3*}6ANI) and T$^{\bullet}$, although overcome by the exchange coupling between the two, contaminates and mixes the D_2 and Q_2 states. In particular, the ZFS term of triplets

$$H_{ZFS} = D(S_z^2 - {}^1/_3S^2) + E(S_x^2 - S_y^2) = D(S_z^2 - {}^1/_3S^2) + {}^1/_2E(S_+^2 + S_-^2) \qquad (8)$$

contains the double-quantum terms S_+^2 and S_-^2 when the triplet is localized and E is significant.

From the experimental point of view, in all the above delocalized triplet-radical systems, the T$^{\bullet}$ radical exhibits a switch in the sign of the polarization as a function of time following photoexcitation, but in our case, we see only a single rise and decay with the sign of the polarization maintained. The experimental observation that generation of the dynamic spin polarization on T$^{\bullet}$ is synchronous with the decay of the polarization of the charge-separated state suggests that the recombinant local triplet ^{3*}NI or ^{3*}6ANI is responsible for the generation of net polarization. This can be explained by the fact that the two ZFS terms S_+^2 and S_-^2 in eq 8 couple the $|D_2 - 1/2\rangle$ sublevel, populated from the D_1 and D_1' states and the vacant $|Q_2 + 3/2\rangle$ sublevel due to their proximity in energy.[90,91,96] Consequently, a net emissive polarization suggests that the energy level of Q_2 lies below D_2, corresponding to an antiferromagnetic coupling between ^{3*}NI (or ^{3*}6ANI) and T$^{\bullet}$, so that $|D_2 - 1/2\rangle$ gets depopulated by the S_+^2 term before the ground D_0 state inherits this spin polarization from D_2 and remains polarized until spin−lattice relaxation destroys the polarization. Specifically, for **3b**/**4b**, the broad signal centered at $g = 2.000$ (Figure 6) is assigned to the emissively polarized D_2 state, because the outer two transitions of the Q_2 state are averaged out during tumbling in solution and its inner transition is not polarized, according to the above analysis. This designation is also supported by the fact that the decay rate of D_2 matches closely the rise of the polarized D_0 state; see Figure 7B. In the cases of **1b** or **2b**, the D_2 signal is covered by the intense D_0 or RP peaks and is not resolved.

Conclusions

In this study of four linear donor−chromophore−acceptor−radical molecules, we observed significant modulation of the lifetimes of the photogenerated triradical states MeOAn$^{+\bullet}$−6ANI−Ph$_n$−A$^{-\bullet}$−T$^{\bullet}$ vs their two-spin counterparts MeOAn$^{+\bullet}$−6ANI−Ph$_n$−A$^{-\bullet}$, where A = NI or PI and $n = 0$ or 1. We rationalize this effect as due to spin catalysis using a model in which the triradical intermediates and the more stable recom-

bination products belong to different spin spaces and the CR processes are accompanied by switching of the spin basis set. From a different point of view, the presence of $T^{\bullet}$ does not alter the driving force for CR but rather loosens the conventional selection rules and opens new pathways of CR. Depending on the rate of CR through these new pathways, the overall CR rate is either faster or slower than the corresponding rates for molecules lacking $T^{\bullet}$. Given the rich information on energetics, kinetics, and polarization obtained from the magnetic field effect and time-resolved EPR experiments, we are able to elucidate the spin dynamics of the triradical state and other photogenerated, spin-polarized intermediates. These results combine to further our understanding of the photochemistry of these novel electron-transfer systems.

Acknowledgment. The work was supported by the National Science Foundation under Grant No. CHE-0415730 and by DARPA. E.A.W. thanks the Graduate School of Northwestern University for a fellowship. E.T.C. thanks the Natural Sciences and Engineering Research Council of Canada (NSERC). The Bruker E580 spectrometer was purchased with partial support from NSF Grant No. CHE-0131048.

Appendix

Spin wave functions of the states shown in Figure 8 are listed below

$$|Q_1 + 3/2\rangle = |\uparrow\uparrow\uparrow\rangle$$

$$|Q_1 - 3/2\rangle = |\downarrow\downarrow\downarrow\rangle$$

$$|Q_1 + 1/2\rangle = (|\uparrow\uparrow\downarrow\rangle + |\uparrow\downarrow\uparrow\rangle + |\downarrow\uparrow\uparrow\rangle)/\sqrt{3}$$

$$|Q_1 - 1/2\rangle = (|\downarrow\downarrow\uparrow\rangle + |\downarrow\uparrow\downarrow\rangle + |\uparrow\downarrow\downarrow\rangle)/\sqrt{3}$$

$$|Q_2\rangle = |Q_1\rangle$$

$$|D_1' + 1/2\rangle = [2|\downarrow(\uparrow\uparrow)\rangle - |\uparrow(\uparrow\downarrow)\rangle - |\uparrow(\downarrow\uparrow)\rangle]/\sqrt{6}$$

$$|D_1' - 1/2\rangle = [2|\uparrow(\downarrow\downarrow)\rangle - |\downarrow(\uparrow\downarrow)\rangle - |\downarrow(\downarrow\uparrow)\rangle]/\sqrt{6}$$

$$|D_1 + 1/2\rangle = [|\uparrow(\uparrow\downarrow)\rangle - |\uparrow(\downarrow\uparrow)\rangle]/\sqrt{2}$$

$$|D_1 - 1/2\rangle = [|\downarrow(\uparrow\downarrow)\rangle - |\downarrow(\downarrow\uparrow)\rangle]/\sqrt{2}$$

$$|D_2 + 1/2\rangle = [2|(\uparrow\uparrow)\downarrow\rangle - |(\uparrow\downarrow)\uparrow\rangle - |(\downarrow\uparrow)\uparrow\rangle]/\sqrt{6}$$

$$|D_2 - 1/2\rangle = [2|(\downarrow\downarrow)\uparrow\rangle - |(\uparrow\downarrow)\downarrow\rangle - |(\downarrow\uparrow)\downarrow\rangle]/\sqrt{6}$$

$$|D_0 + 1/2\rangle = [|(\uparrow\downarrow)\uparrow\rangle - |(\downarrow\uparrow)\uparrow\rangle]/\sqrt{2}$$

$$|D_0 - 1/2\rangle = [|(\uparrow\downarrow)\downarrow\rangle - |(\downarrow\uparrow)\downarrow\rangle]/\sqrt{2}$$

In these spin wave functions, the three spins listed from left to right in each term are the unpaired spin at, or transferred from, the $MeOAn^{+\bullet}$, $A^{-\bullet}$, and $T^{\bullet}$ moieties, respectively. The dominant couplings are emphasized with parentheses.

Supporting Information Available: Synthesis and characterization details for all new compounds, calculations of energetics, as well as femtosecond transient absorption kinetics are available in the Supporting Information. This material is available free of charge via the Internet at http://pubs.acs.org.

References and Notes

(1) Wasielewski, M. R. *Chem. Rev.* **1992**, *92*, 435−461.
(2) Gust, D.; Moore, T. A.; Moore, A. L. *Acc. Chem. Res.* **2001**, *34*, 40−48.
(3) Wagner, R. W.; Lindsey, J. S.; Seth, J.; Palaniappan, V.; Bocian, D. F. *J. Am. Chem. Soc.* **1996**, *118*, 3996−3997.
(4) de Silva, A. P.; Gunaratne, H. Q. N.; Gunnlaugsson, T.; Huxley, A. J. M.; McCoy, C. P.; Rademacher, J. T.; Rice, T. E. *Chem. Rev.* **1997**, *97*, 1515−1566.
(5) Willner, I.; Willner, B. *J. Mater. Chem.* **1998**, *8*, 2543−2556.
(6) Tour, J. M.; Kozaki, M.; Seminario, J. M. *J. Am. Chem. Soc.* **1998**, *120*, 8486−8493.
(7) Collier, C. P.; Mattersteig, G.; Wong, E. W.; Luo, Y.; Beverly, K.; Sampaio, J.; Raymo, F. M.; Stoddart, J. F.; Heath, J. R. *Science* **2000**, *289*, 1172−1175.
(8) Davis, W. B.; Svec, W. A.; Ratner, M. A.; Wasielewski, M. R. *Nature* **1998**, *396*, 60−63.
(9) Waldeck, D. H.; Beratan, D. N. *Science* **1993**, *261*, 576−577.
(10) Metzger, R. M. *Acc. Chem. Res.* **1999**, *32*, 950−957.
(11) Chen, J.; Reed, M. A.; Rawlett, A. M.; Tour, J. M. *Science* **1999**, *286*, 1550−1552.
(12) Prathapan, S.; Yang, S. I.; Seth, J.; Miller, M. A.; Bocian, D. F.; Holten, D.; Lindsey, J. S. *J. Phys. Chem. B* **2001**, *105*, 8237−8248.
(13) Yang, S. I.; Prathapan, S.; Miller, M. A.; Seth, J.; Bocian, D. F.; Lindsey, J. S.; Holten, D. *J. Phys. Chem. B* **2001**, *105*, 8249−8258.
(14) Yang, S. I.; Lammi, R. K.; Prathapan, S.; Miller, M. A.; Seth, J.; Diers, J. R.; Bocian, D. F.; Lindsey, J. S.; Holten, D. *J. Mater. Chem.* **2001**, *11*, 2420−2430.
(15) del Rosario Benites, M.; Johnson, T. E.; Weghorn, S.; Yu, L. H.; Rao, P. D.; Diers, J. R.; Yang, S. I.; Kirmaier, C.; Bocian, D. F.; Holten, D.; Lindsey, J. S. *J. Mater. Chem.* **2002**, *12*, 65−80.
(16) Jones, B. A.; Ahrens, M. J.; Yoon, M. H.; Facchetti, A.; Marks, T. J.; Wasielewski, M. R. *Angew. Chem., Int. Ed.* **2004**, *43*, 6363−6366.
(17) Gosztola, D.; Niemczyk, M. P.; Wasielewski, M. R. *J. Am. Chem. Soc.* **1998**, *120*, 5118−5119.
(18) Hayes, R. T.; Wasielewski, M. R.; Gosztola, D. *J. Am. Chem. Soc.* **2000**, *122*, 5563−5567.
(19) Lukas, A. S.; Wasielewski, M. R. In *Molecular switches*; Feringa, B. L., Ed.; Wiley-VCH: Weinheim, Germany, 2001; pp 1−35.
(20) Prisner, T.; Dobbert, O.; Dinse, K. P.; Van Willigen, H. *J. Am. Chem. Soc.* **1988**, *110*, 1622−1623.
(21) Angerhofer, A.; Toporowicz, M.; Bowman, M. K.; Norris, J. R.; Levanon, H. *J. Phys. Chem.* **1988**, *92*, 7164−7166.
(22) Rajca, A. *Chem. Rev.* **1994**, *94*, 871−893.
(23) Nakatsuji, S.; Anzai, H. *J. Mater. Chem.* **1997**, *7*, 2161−2174.
(24) Lahti, P. M., Ed. *Magnetic properties of organic materials*; Marcel Dekker: New York, 1999.
(25) Crayston, J. A.; Devine, J. N.; Walton, J. C. *Tetrahedron* **2000**, *56*, 7829−7857.
(26) Sugawara, T.; Sakurai, H.; Izuoka, A. In *Hyper-structured molecules II: chemistry, physics and applications*; Sasabe, H., Ed.; Gordon and Breach: Amsterdam, The Netherlands, 2001; pp 35−57.
(27) Wolf, S. A.; Awschalom, D. D.; Buhrman, R. A.; Daughton, J. M.; von Molnar, S.; Roukes, M. L.; Chtchelkanova, A. Y.; Treger, D. M. *Science* **2001**, *294*, 1488−1495.
(28) Miller, J. S.; Manson, J. L. *Acc. Chem. Res.* **2001**, *34*, 563−570.
(29) Awschalom, D. D.; Flatte, M. E.; Samarth, N. *Sci. Am.* **2002**, *286*, 66−73.
(30) Rajca, A. *Chem.−Eur. J.* **2002**, *8*, 4834−4841.
(31) Itkis, M. E.; Chi, X.; Cordes, A. W.; Haddon, R. C. *Science* **2002**, *296*, 1443−1445.
(32) Buchachenko, A. L.; Berdinsky, V. L. *Chem. Rev.* **2002**, *102*, 603−612.
(33) Buchachenko, A. L.; Ruban, L. V.; Step, E. N.; Turro, N. J. *Chem. Phys. Lett.* **1995**, *233*, 315−318.
(34) Vlassiouk, I.; Smirnov, S.; Kutzki, O.; Wedel, M.; Montforts, F.-P. *J. Phys. Chem. B* **2002**, *1−6*, 8657−8666.
(35) Smirnov, S.; Vlassiouk, I.; Kutzki, O.; Wedel, M.; Montforts, F.-P. *J. Am. Chem. Soc.* **2002**, *124*, 4212−4213.
(36) Volkova, O. S.; Taraban, M. B.; Plyusnin, V. F.; Leshina, T. V.; Egorov, M. P.; Nefedov, O. M. *J. Phys. Chem. A* **2003**, *107*, 4001−4005.
(37) Mori, Y.; Sakaguchi, Y.; Hayashi, H. *J. Phys. Chem. A* **2002**, *106*, 4453−4467.
(38) Mori, Y.; Sakaguchi, Y.; Hayashi, H. *Bull. Chem. Soc. Jpn.* **2001**, *74*, 293−304.
(39) Ishii, K.; Hirose, Y.; Kobayashi, N. *J. Phys. Chem. A* **1999**, *103*, 1986−1990.
(40) Ishii, K.; Hirose, Y.; Fujitsuka, M.; Ito, O.; Kobayashi, N. *J. Am. Chem. Soc.* **2001**, *123*, 702−708.
(41) Weiss, E. A.; Chernick, E. T.; Wasielewski, M. R. *J. Am. Chem. Soc.* **2004**, *126*, 2326−2327.

(42) Forrester, A. R.; Hay, J. M.; Thomson, R. H. *Organic chemistry of stable free radicals*; Academic Press: London, 1968.
(43) Sümmermann, W.; Deffner, U. *Tetrahedron* **1975**, *31*, 593−596.
(44) Greenfield, S. R.; Svec, W. A.; Gosztola, D.; Wasielewski, M. R. *J. Am. Chem. Soc.* **1996**, *118*, 6767−6777.
(45) Weiss, E. A.; Ratner, M. A.; Wasielewski, M. R. *J. Phys. Chem. A* **2003**, *107*, 3639−3647.
(46) Hasharoni, K.; Levanon, H.; Greenfield, S. R.; Gosztola, D. J.; Svec, W. A.; Wasielewski, M. R. *J. Am. Chem. Soc.* **1995**, *117*, 8055−8056.
(47) Hasharoni, K.; Levanon, H.; Greenfield, S. R.; Gosztola, D. J.; Svec, W. A.; Wasielewski, M. R. *J. Am. Chem. Soc.* **1996**, *118*, 10228−10235.
(48) Lukas, A. S.; Miller, S. E.; Wasielewski, M. R. *J. Phys. Chem. B* **2000**, *104*, 931−940.
(49) Giaimo, J. M.; Gusev, A. V.; Wasielewski, M. R. *J. Am. Chem. Soc.* **2002**, *124*, 8530−8531.
(50) Yamaguchi, S.; Hamaguchi, H. O. *Appl. Spectrosc.* **1995**, *49*, 1513−1515.
(51) Schweiger, A. Jeschke, G. *Principles of pulse electron paramagnetic resonance*; Oxford University Press: Oxford, U.K., 2001.
(52) Debreczeny, M. P.; Svec, W. A.; Marsh, E. M.; Wasielewski, M. R. *J. Am. Chem. Soc.* **1996**, *118*, 8174−8175.
(53) Gosztola, D.; Niemczyk, M. P.; Svec, W. A.; Lukas, A. S.; Wasielewski, M. R. *J. Phys. Chem. A* **2000**, *104*, 6545−6551.
(54) Weiss, E. A.; Sinks, L. E.; Lukas, A. S.; Chernick, E. T.; Ratner, M. A.; Wasielewski, M. R. *J. Phys. Chem. B* **2004**, *108*, 10309−10316.
(55) Lukas, A. S.; Bushard, P. J.; Weiss, E. A.; Wasielewski, M. R. *J. Am. Chem. Soc.* **2003**, *125*, 3921−3930.
(56) Mori, Y.; Sakaguchi, Y.; Hayashi, H. *Chem. Phys. Lett.* **1998**, *286*, 446−451.
(57) Shaakov, S.; Galili, T.; Stavitski, E.; Levanon, H.; Lukas, A.; Wasielewski, M. R. *J. Am. Chem. Soc.* **2003**, *125*, 6563−6572.
(58) Duling, D. R. *J. Magn. Reson. B* **1994**, *104*, 105−110.
(59) Carrington, A.; McLachlan, A. D. *Introduction to magnetic resonance with applications to chemistry and chemical physics*; Harper and Row: New York, 1967.
(60) Corvaja, C.; Maggini, M.; Prato, M.; Scorrano, G.; Venzin, M. *J. Am. Chem. Soc.* **1995**, *117*, 8857−8858.
(61) Yamauchi, S. *Bull. Chem. Soc. Jpn.* **2004**, *77*, 1255−1268.
(62) McCain, D. C. *J. Magn. Reson.* **1972**, *7*, 170−176.
(63) McLauchlan, K. A. In *Modern pulsed and continuous-wave electron spin resonance*; Kevan, L.; Bowman, M. K., Eds.; Wiley: New York, 1990; pp 285−363.
(64) Hasharoni, K.; Levanon, H.; Tang, J.; Bowman, M. K.; Norris, J. R.; Gust, D.; Moore, T. A.; Moore, A. L. *J. Am. Chem. Soc.* **1990**, *112*, 6477−6481.
(65) Timmel, C. R.; Hore, P. J. *Chem. Phys. Lett.* **1994**, *226*, 144−150.
(66) Weis, V.; van Willigen, H. *J. Porphyrins Phthalocyanines* **1998**, *2*, 353−361.
(67) Eaton, S. S.; Eaton, G. R. *Biol. Magn. Reson.* **2000**, *19*, 29−154.
(68) Fujisawa, J.; Ishii, K.; Ohba, Y.; Yamauchi, S.; Fuhs, M.; Möbius, K. *J. Phys. Chem. A* **1999**, *103*, 213−216.
(69) Ishii, K.; Fujisawa, J.; Ohba, Y.; Yamauchi, S. *J. Am. Chem. Soc.* **1996**, *118*, 13079−13080.
(70) Haberkorn, R.; Michel-Beyerle, M. E. *Biophys. J.* **1979**, *26*, 489−498.
(71) Hoff, A. J.; Rademaker, H.; Van Grondelle, R.; Duysens, L. N. M. *Biochim. Biophys. Acta* **1977**, *460*, 547−554.
(72) Mori, Y.; Sakaguchi, Y.; Hayashi, H. *J. Phys. Chem. A* **2000**, *104*, 4896−4905.
(73) Till, U.; Hore, P. J. *Mol. Phys.* **1997**, *90*, 289−296.
(74) Wegner, M.; Fischer, H.; Grosse, S.; Vieth, H. M.; Oliver, A. M.; Paddon-Row, M. N. *Chem. Phys.* **2001**, *264*, 341−353.
(75) Weller, A.; Staerk, H.; Treichel, R. *Faraday Discuss.* **1984**, *78*, 271−278.
(76) Marcus, R. A. *J. Chem. Phys.* **1956**, *24*, 966−978.
(77) Kobori, Y.; Kawai, A.; Obi, K. *J. Phys. Chem.* **1994**, *98*, 6425−6429.
(78) Wiederrecht, G. P.; Svec, W. A.; Wasielewski, M. R.; Galili, T.; Levanon, H. *J. Am. Chem. Soc.* **2000**, *122*, 9715−9722.
(79) Marcus, R. A. *J. Chem. Phys.* **1965**, *43*, 679−701.
(80) Weiss, E. A.; Tauber, M. J.; Ratner, M. A.; Wasielewski, M. R. *J. Am. Chem. Soc.* **2005**, *127*, 6052−6061.
(81) Dupeyre, R. M.; Lemaire, H.; Rassat, A. *J. Am. Chem. Soc.* **1965**, *87*, 3771−3772.
(82) Molecular geometries are modeled at the UHF/PM3 level, using HyperChem; Hypercube, Inc.: Gainesville, FL.
(83) Closs, G. L.; Forbes, M. D. E.; Norris, J. R. *J. Phys. Chem.* **1987**, *91*, 3592−3599.
(84) Hoytink, G. J. *Acc. Chem. Res.* **1969**, *2*, 114−120.
(85) Jortner, J. *J. Chem. Phys.* **1976**, *64*, 4860−4867.
(86) Weiss, E. A.; Ahrens, M. J.; Sinks, L. E.; Ratner, M. A.; Wasielewski, M. R. *J. Am. Chem. Soc.* **2004**, *126*, 9510−9511.
(87) Muus, L. T.; Atkins, P. W.; McLauchlan, K. A.; Pedersen, J. B. *Chemically induced magnetic polarization*; Reidel: Dordrecht, The Netherlands, 1977.
(88) Norris, J. R.; Morris, A. L.; Thurnauer, M. C.; Tang, J. *J. Chem. Phys.* **1990**, *92*, 4239−4249.
(89) Blattler, C.; Jent, F.; Paul, H. *Chem. Phys. Lett.* **1990**, *166*, 375−380.
(90) Kawai, A.; Okutsu, T.; Obi, K. *J. Phys. Chem.* **1991**, *95*, 9130−9134.
(91) Goudsmit, G. H.; Paul, H.; Shushin, A. I. *J. Phys. Chem.* **1993**, *97*, 13243−13249.
(92) Blank, A.; Levanon, H. *J. Phys. Chem. A* **2001**, *105*, 4799−4807.
(93) Gast, P.; Hoff, A. J. *Biochim. Biophys. Acta* **1979**, *548*, 520−535.
(94) Hoff, A. J.; Gast, P. *J. Phys. Chem.* **1979**, *83*, 3355−3358.
(95) Conti, F.; Corvaja, C.; Gattazzo, C.; Toffoletti, A.; Bergo, P.; Maggini, M.; Scorrano, G.; Prato, M. *Phys. Chem. Chem. Phys.* **2001**, *3*, 3526−3531.
(96) Kobori, Y.; Takeda, K.; Tsuji, K.; Kawai, A.; Obi, K. *J. Phys. Chem. A* **1998**, *102*, 5160−5170.